Proprioceptive feedback design for gait synchronization in collective undulatory robots

Zhuonan Hao, Wei Zhou & Nick Gravish

View supplementary material

Published online: 04 Apr 2022.

Submit your article to this journal

View related articles

View Crossmark data

RSJ   Taylor & Francis
        Taylor & Francis Group

Check for updates

FULL PAPER

Proprioceptive feedback design for gait synchronization in collective undulatory robots

Zhuonan Hao ⬡, Wei Zhou ⬡ and Nick Gravish ⬡

Department of Mechanical and Aerospace Engineering, University of California San Diego, La Jolla, CA, USA

ABSTRACT

The collective movement of animals has long been a source of inspiration for multi-agent swarm robotics. One of the fundamental goals for swarm robotics study is to understand how effective and robust collective behaviors can emerge from simple interaction principles. When animal or robot collectives are in high-density configurations the ability for visual or auditory sensing is diminished and the opportunities for interacting through mechanical contact are enhanced. In this paper, we study how robots that move through lateral body undulation in close proximity are capable of synchronizing their oscillatory gaits through contact interactions between adjacent robots. Critically, gait phase synchronization occurs without the requirement for robot–robot communication, and instead can be engineered as an emergent property of the robot control system. We present a proprioceptive feedback control system that generates collective gait phase synchronization of undulatory robots in experiment and simulation. We first validate this control system using a simple one-dimensional toy model to demonstrate how proprioceptive feedback governs phase synchronization. Simulations and experiments with undulatory three-link robots further demonstrate how phase synchronization can be controlled. Lastly, we demonstrate that robot pairs moving in a confined tunnel can synchronize their movements which leads to faster group locomotion through confined spaces.

1. Introduction

Coordination of collective motion in robot groups is a fundamental challenge in swarm robotics [1]. Centralized approaches to the planning and control of collective motion require long-range communication and perception capabilities among robots, so that a central planning system can plan the motion of the group. Alternatively, decentralized control approaches rely on motion planning algorithms that run independently on each robot based on local information exchange between robots. However, in many of the established approaches for multi-robot control the robots exchange information through sensors and communication protocols. In this paper, we explore an example of emergent collective robot motion in which no information is exchanged and instead robots act only on internal state sensing, called proprioception. Through the appropriate design of control feedback, we are able to generate undulatory snake-like robot collectives that synchronize the phases of their undulatory gaits when in close proximity.

Synchronization of movement is a common collective behavior in many biological systems. For example, many swimming microorganisms are capable of synchronizing their body or appendage motion by interacting with their neighbors through fluidic forces. Recent studies suggest that both long-range hydrodynamic interactions [2,3] and short-range contact interactions [4,5] can bring about the stable, synchronized collective motions in these systems. For small organisms such as bacteria, the synchronized motion of cilia [6], and flagella [7] are driven by fluid–mechanical interactions. However, in larger organisms such as the worm *C. elegans* hydrodynamic interactions are less important, and instead, interaction through contact becomes the predominant factor for gait synchronization [8]. Even for smaller systems, mechanical contact interactions may be of importance in high-density population scenario [9].

The work presented here is inspired by the collective undulatory synchronization observed in groups of swimming worms [8,10]. *C. elegans* is observed to produce undulatory movements by a propagating sinusoidal wave, traveling from head to tail [11]. Recent studies have determined that intermittent mechanical contact is responsible for synchronization of the undulatory gaits of worm groups [8]. Biomechanical and neural experiments have demonstrated that the generation of

---

undulatory body motion is largely through local proprioceptive reflex responses along the body that sense the local body bending and generate a bending actuation in response [12,13]. Thus the body bending wave propagation occurs as a 'reflex chain' in which the wave propagation doesn't involve communication between oscillators and instead responds only to the bending state of the local body region. Experiments have demonstrated this local oscillator principle by isolating body regions and showing that a propagating wave is halted at a body region where bending is inhibited [12]. In the work proposed in this paper, we will include oscillator coupling terms to enforce the generation of traveling wave, however, the gait phase synchronization will occur through proprioceptive reflex responses in the joint controller.

In the following work, we will demonstrate theoretically and experimentally that oscillators with only proprioceptive feedback can enable synchronization of robot gaits through intermittent contact. We further demonstrate how an inhibitory versus excitatory proprioceptive gain controls whether robots synchronize to in-phase versus opposite-phase motion. We lastly show how this is useful for emergent coordination of snake-like robots to traverse narrow gaps. This work is presented through a combination of analysis, simulation, and experiment. Ultimately we demonstrate that synchronization of undulatory gaits can be designed and is beneficial for small groups of robots to traversal narrow and confined environments.

2. A brief background on nonlinear oscillators and synchronization

The mathematical framework for designing and analyzing the synchronization of undulatory locomotion relies on the study of nonlinear oscillators. An oscillator is an autonomous dynamical system which exhibits a stable limit cycle attractor [14,15]. A stable limit cycle is a closed trajectory in the phase-space of the dynamical system in which a surrounding region of initial conditions is attracted onto the limit cycle. The closed trajectory of the limit cycle implies that the system's state variables will be periodic, i.e. the system in steady state will oscillate.

Nonlinear oscillators have been extensively used in the robotics field for generating stable periodic motion trajectories of joints and bodies [14,16–19]. Limit cycles are advantageous because: (a) the systems can produce the periodic oscillations spontaneously without time-dependent forcing, (b) the oscillation amplitude is robust and resistant against transient perturbation with asymptotic return to the limit cycle, and (c) the oscillation phase is marginally stable enabling phase perturbations to persist. It is this last point which allows for phase

synchronization between oscillators. Limit cycle control of walking, swimming, and hopping robots have demonstrated the robustness of these control methods in addition to novel adaptive behaviors which can adjust to changing loads, environmental forces, and behaviors [20–23].

In seminal work from Buchli, Righetti, and Ijspeert, these authors introduced a principled approach to designing dynamical systems that generate limit cycle behavior for robot control [14]. The core of this method is to work from a phase-radius coordinate system (PRCS) approach for designing limit cycle behavior. For a second-order dynamical system, the phase-radius coordinate system effectively converts from the phase-space (which are the equivalent Cartesian coordinates of the phase space) to a polar coordinate form. Thus with the appropriate rescaling of phase along the limit cycle (see [14] for details), a PRCS limit cycle can be written as

$$\dot{\phi} = \omega \tag{1}$$

$$\dot{\mathbf{r}} = \mathbf{F}(\mathbf{r}) \tag{2}$$

where ϕ is the evolution of phase along the limit cycle trajectory and $\mathbf{r}$ is the radial distance from the origin to the instantaneous system state (which can be high-dimensional). The phase of an oscillator has a strict definition that it must be a quantity that increases at constant rate. In this work, we will use a slightly less strict definition of phase which will be described in the next section. The PRCS concept is advantageous because the desired limit cycle behavior of the system is the starting point for feedback design, and the PRCS system can eventually be recast into the desired phase-space coordinates as necessary. Similarly, other dynamical systems can be converted into PRCS for analysis of limit-cycle behavior.

When multiple limit cycle oscillators are coupled, the neutral stability of the phase variable can lead to synchronization phenomena [24]. Phase synchronization occurs when oscillators with a common frequency align their phases in often an in-phase, or anti-phase, arrangement. If oscillators have different natural frequencies, in some instances coupling can drive the group to a common oscillatory frequency. The canonical model for such synchronizing systems is the Kuramoto model of synchronization [25] where the phase variables of oscillators are directly coupled. In the appropriate regimes of coupling strength and connectivity, this system will display a wide range of phase and frequency synchronization behavior. The Kuramoto system has been extensively studied and there are many reviews of the system phenomenology [26]. However, we note that a critical component of synchronization in the Kuramoto system is the explicit coupling between oscillator phases. Oscillator i must have information about oscillator j to determine the relative

phase difference. This is in contrast to the method we will present in the next section which does not rely on shared information across oscillators.

3. An illustrative model for phase synchronization through proprioceptive feedback control

3.1. Model definition and collision dynamics

Our ultimate goal is to develop a feedback control system for the joints on an undulatory snake-like robot that enables synchronization with other robots through intermittent contact. In this section, we envision the contact interactions between two 'body elements' of adjacent robots who's lateral movement are governed by a proprioceptive feedback law. From this toy model, we will study the process of phase synchronization and we will mathematically validate the phase convergence properties of the proposed control framework. Lastly we will introduce the concept of a contact-to-contact return map which will be used to evaluate the phase adaption process here, and which we will return to for analysis of multi-link robots.

We reduce the interaction between two snake-like robots into two contact-coupled body elements ('blocks') that oscillate laterally in one dimension (Figure 1 a). The block lateral positions are given by x_1 and x_2 and for simplicity we assume the blocks are zero-width (i.e. points). The oscillatory motion of positions (x_1, x_2) are governed by a phase oscillator which has frequency ω, and an adaptive feedback gain and proprioception function given by γ and $g(\phi_{m,i}, \phi_i)$ respectively

$$\dot{\phi}_i = \omega + \gamma \, g(\phi_{m,i}, \phi_i) \tag{3}$$

Critically, the proprioception feedback function only takes into account each block's individual controller phase ϕ_i and the instantaneous measured phase through proprioception $\phi_{m,i}$. We note that our definition of phase is less strict than introduced in the previous section. We refer to phase as the polar angle between the origin and the current state in the phase-space. In the absence of contact, the phase oscillator generates a constant phase velocity, and we map the controller phase to the lateral motion of the blocks in physical space through the commanded position

$$\tilde{x}_1 = R \cos(\phi_1) - \frac{\delta}{2}$$
$$\tilde{x}_2 = R \cos(\phi_2) + \frac{\delta}{2} \tag{4}$$

where the offset δ accounts for the separation of the equilibrium oscillation point between the two blocks (i.e. the lateral separation distance between the midline of two undulating robots). We note that when a collision between blocks occurs the commanded position and actual position will not be equal, $\tilde{x}_i \neq x_i$.

3.2. Modeling contact interactions

Now that we have defined the phase dynamics equation (3) and their mapping to spatial position equation (4), we motivate a convenient geometric visualization of the block interactions. In Figure 1(b), we show two circular limit cycles with radius R and centered on the x-locations $\pm\frac{\delta}{2}$. The oscillator's phase, ϕ_i, is given by the angle from the x-axis to the controller's location on the limit cycle trajectory. In the absence of contact, the instantaneous spatial position of each block is simply the projection of the instantaneous controller phase onto the x-axis (Equation 4). The blocks will collide with each other when the position condition is met

$$R \cos(\phi_1) - R \cos(\phi_2) = \delta \tag{5}$$

When the blocks make contact with each other, we assume that they both come to rest in contact ($\dot{x}_i = 0$). We denote with the superscript $\pm$ the values of a variable instantaneously before ($-$) and after ($+$) contact, thus the controller phases immediately before contact are ϕ_i^- for example. During contact the controller phases will evolve according to Equation (3) while the blocks themselves are motionless. The relative phase difference $\Delta\phi = \phi_1 - \phi_2$ determines the phase convergence properties of a contact interaction with the most critical value being the difference in phase between pre and post contact, $\Delta\phi^+ - \Delta\phi^-$ (Figure 1c).

To model the control behavior during contact we make several very simple assumptions about the contact interaction between blocks: (1) while in contact the blocks remain motionless and remain at positions determined by Equations (4) for the phases ϕ_i^-, (2) the blocks will remain in contact as long as their commanded positions cause them to push against each other, and (3) the blocks will lose contact and begin moving again when the commanded position results in a separation. Figure 1(d) shows an example of this process: Step (1) before contact the positions are governed by Equation (4). In steps (2)–(3), the blocks make contact and their velocity drops to zero. The controller phase continues to evolve around the limit cycle governed by Equation (3). Since the block on the left (red) is commanded to move to the right and the block on the right (blue) is commanded to move left, the blocks maintain pushing contact against each other and are motionless. However, at step (4) the phase of the right block finally reaches a value which causes the commanded position to begin pulling away from the contact location (the blue block moves to the right), this releases the contact interaction between the blocks and they will
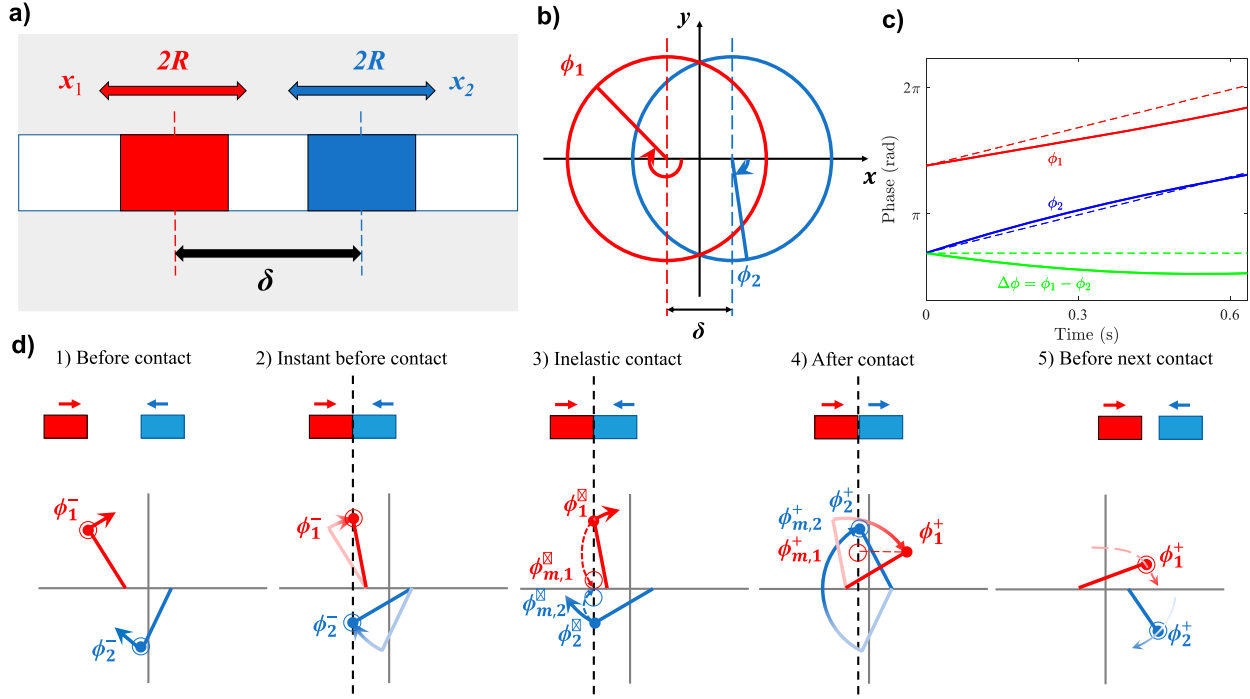
Figure 1. The phase oscillator model for the synchronization of contact-coupled blocks. (a) Two blocks are initially configured by separation distance δ and perform horizontal harmonic motion around the respective equilibrium points (dashed line). (b) The limit cycle schematic illustration of the oscillator interaction process. (c) The phase adaption effect emerges during the contact duration. The plot compares the phase evolution under different actuation schemes (solid line: with feedback, dashed line: without feedback). (d) The complete contact course is shown in steps 1–5 (circled and solid points indicated the measured and internal phases respectively): (1) Two oscillators are at initial phase difference $\Delta^- = \phi_1^- - \phi_2^-$. (2) Oscillators start contact when position overlapping. (3) Inelastic contact leads velocities to drop to 0 instantaneously. Measured phase $\phi_{m,1}$ and $\phi_{m,2}$ changes accordingly. (4) Oscillators stop interaction when satisfying separation conditions. (5) Oscillators continue evolving until contact again and keep repeating steps 1–5 before synchronization.

move according to the oscillator controller and spatial mapping equations.

The loss of contact condition can be easily determined through the geometry of the limit cycles. The block whose position is closer to zero before contact is the obstructing block (e.g. the blue block in Figure 1 d). The obstructing block will keep obstructing until its controller phase reaches a value of ϕ_i^+ determined by the condition $\cos(\phi_i^-) = \cos(\phi_i^+)$ and $\sin(\phi_i^-) = -\sin(\phi_i^+)$. In words, this condition is when the controller phase causes the obstructing block to move from its current position in the opposite direction of the pre-collision velocity. For the example in Figure 1(d), this can be written as the geometric relationship $\phi_2^+ = 2\pi - \phi_2^-$. The above rules describe a simple process wherein two bodies controlled by position controlled servos will come into contact and remain contact until one is commanded to pull away.

3.3. Proprioceptive feedback and measured phase

In this section, we now turn to the proprioceptive feedback law, $\gamma g(\phi_{m,i}, \phi_i)$, and the measured phase $\phi_{m,i}$ of

Equation (3). In the absence of a collision the motion of the blocks will exactly track the commanded motion, and we thus assume that the measured phase, $\phi_{m,i}$, is equal to the instantaneous controller phase ϕ_i. However, when a collision occurs the blocks will come to rest and the instantaneous phase will differ from the actual measured phase of the blocks based off of their spatial kinematics. We assume that spatial kinematics state is governed by position (x_i) and velocity (the y_i axis, although this does not hold generally for the experimental system). Thus the measured phase can be determined by the angle generated from the equation

$$\phi_{m,i} = \arctan\left(\frac{y_i}{x_i}\right) \qquad (6)$$

Taking the y-component of the instantaneous state as velocity (which does not hold generally for PRCS systems) then after a collision both velocities go to zero, and thus $y_i = 0$. This results in a measured phase of $\phi_{m,i} = \{0, \pi\}$ depending on which quadrant the collision occurs in. In the example of Figure 1(d), both measured phases go to $\phi_{m,1} = \phi_{m,2} = \pi$.

Our goal is to choose an appropriate proprioceptive feedback function which can ensure that the limit cycle oscillators converge to phase synchronization. Thus during a collision the oscillator ahead in phase should be slowed and the oscillator behind in phase should be sped up. A simple candidate proprioceptive feedback law that achieves this behavior is $g(\phi_{m,i}, \phi_i) = \sin(\phi_{m,i} - \phi_i)$. This yields the overall phase oscillator controller

$$\dot{\phi}_i = \omega + \gamma \sin\left(\phi_{m,i} - \phi_i\right) \tag{7}$$

In the example of Figure 1 the red block is ahead in phase, and the blue is behind ($\phi_1 > \pi > \phi_2$). Once both measured phases $\phi_{m,i} = 0$ the proprioceptive feedback function becomes $\sin(\pi - \phi_i)$ which simplifies to $\sin(\phi_i)$. During the collision, the oscillator ahead ($\phi_1 > \pi$) has a phase rate that is slowed ($\sin(\phi_1) < 0$), while the oscillator behind ($\phi_2 < \pi$) in phase has a phase rate that is increased ($\sin(\phi_2) > 0$). Thus we propose that this proprioceptive feedback law will result in phase synchronization for a pair of laterally undulating one-dimensional blocks.

Figure 1(c) shows an example of phase change during a single contact event. The contact-coupled blocks start with initial phase difference $\Delta\phi^-$ of 2.16, and a final phase difference of $\Delta\phi^+ = 1.96$ after contact is lost. Iterating this process in the next section will demonstrate that $\Delta\phi$ asymptotically converge to 0 for appropriate proprioception feedback, which indicates the in-phase synchronization.

3.4. Synchronization analysis

We now propose an analytical method to calculate the change in phase difference between the controllers before and after collision. In this example, we will calculate the collision-induced phase change for the case shown in Figure 1(d) in which the right block obstructs the left block. This method, however, is generalizable across any collision condition.

When the blocks first make contact they are at positions $x_1 - x_2 = 0$ yielding $R\cos(\phi_1^-) - R\cos(\phi_2^-) = \delta$. The initial phases at start of collision are denoted by the superscript $^-$. During the collision, the measured phase for each oscillator becomes $\phi_{m,1} = \phi_{m,2} = \pi$ and the phase controllers simplify to

$$\dot{\phi}_1 = \omega + \gamma \sin\phi_1 \tag{8}$$

$$\dot{\phi}_2 = \omega + \gamma \sin\phi_2 \tag{9}$$

These two controller equations are uncoupled and can be integrated directly through separation of variables

$$\int_{\phi_1^-}^{\phi_1^+} \frac{1}{\omega + \gamma \sin\phi_1} \, d\phi_1 = \int_{t^-}^{t^+} dt \tag{10}$$

$$\int_{\phi_2^-}^{\phi_2^+} \frac{1}{\omega + \gamma \sin\phi_2} \, d\phi_2 = \int_{t^-}^{t^+} dt \tag{11}$$

The contact duration $[t^-, t^+]$ is the same for both oscillators and thus we have the equality

$$\int_{\phi_1^-}^{\phi_1^+} \frac{1}{\omega + \gamma \sin\phi_1} \, d\phi_1 = \int_{\phi_2^-}^{\phi_2^+} \frac{1}{\omega + \gamma \sin\phi_2} \, d\phi_2 \tag{12}$$

These two equations have closed form and real integral solutions as long as $\gamma < \omega$

$$\tan^{-1}\left(\frac{\omega \tan\left(\frac{\phi_1^+}{2}\right) + \gamma}{\sqrt{\omega^2 - \gamma^2}}\right) - \tan^{-1}\left(\frac{\omega \tan\left(\frac{\phi_1^-}{2}\right) + \gamma}{\sqrt{\omega^2 - \gamma^2}}\right)$$

$$= \tan^{-1}\left(\frac{\omega \tan\left(\frac{\phi_2^+}{2}\right) + \gamma}{\sqrt{\omega^2 - \gamma^2}}\right)$$

$$- \tan^{-1}\left(\frac{\omega \tan\left(\frac{\phi_2^-}{2}\right) + \gamma}{\sqrt{\omega^2 - \gamma^2}}\right) \tag{13}$$

Since this equation has many repeating terms we define the function

$$\xi(\phi_i^\pm) = \tan^{-1}\left(\frac{\omega \tan\left(\frac{\phi_i^\pm}{2}\right) + \gamma}{\sqrt{\omega^2 - \gamma^2}}\right) \tag{14}$$

We now seek to solve for the unknown final phase ϕ_1^+ in terms of the other phases, which can be determined as

$$\phi_2^+ = 2\pi - \phi_2^- \tag{15}$$

$$\phi_1^- = 2\pi - \cos^{-1}\left(\frac{\delta}{R} + \cos(\phi_2^-)\right) \tag{16}$$

and ϕ_2^- is a known parameter. Substituting Equations (15), (16) into Equation (13) yields

$$\tan^{-1}\left(\frac{\omega \tan\left(\frac{\phi_1^+}{2}\right) + \gamma}{\sqrt{\omega^2 - \gamma^2}}\right) = \xi(2\pi - \phi_2^-) - \xi(\phi_2^-)$$

$$+ \xi\left(2\pi - \cos^{-1}\left(\frac{\delta}{R} + \cos(\phi_2^-)\right)\right) \tag{17}$$

Solving for the only unknown phase, ϕ_1^+ yields

$$\phi_1^+ = 2\tan^{-1}\left(\tan\left(\xi(2\pi - \phi_2^-) - \xi(\phi_2^-)\right.\right.$$

$$\left.\left. + \xi\left(2\pi - \cos^{-1}\left(\frac{\delta}{R} + \cos(\phi_2^-)\right)\right)\right)\sqrt{1 - \left(\frac{\gamma}{\omega}\right)^2} - \frac{\gamma}{\omega}\right) \tag{18}$$

This equation thus provides us with the final phase difference of the oscillators and can be used to solve for the evolution of ϕ_1 and ϕ_2 before and after contact.

Now, we introduce the concept of phase return map, which is an evaluation tool for phase adaption between the two oscillators. In the case of our contact interacting blocks, we have two maps that iterate the phases from the beginning to the end of the two dynamical regimes, in contact and not in contact. The first map, $\mathcal{C}$, is defined by Equations (16) and (18) and maps the controller phases at the beginning of contact to the controller phases at the end of contact

$$\mathcal{C} : \begin{bmatrix} \phi_1^- \\ \phi_2^- \end{bmatrix}_n \rightarrow \begin{bmatrix} \phi_1^+ \\ \phi_2^+ \end{bmatrix}_n \qquad (19)$$

The next map, $\mathcal{D}$, iterates the system through the non-contact regime and determines the phases at the beginning of the next contact from the phases at the end of the previous contact.

$$\mathcal{D} : \begin{bmatrix} \phi_1^+ \\ \phi_2^+ \end{bmatrix}_n \rightarrow \begin{bmatrix} \phi_1^- \\ \phi_2^- \end{bmatrix}_{n+1} \qquad (20)$$

The composition of these two maps yields the collision-to-collision phase, which tells us how the overall phases (and phase difference between the two systems) change from contact to contact

$$\mathcal{R} : \mathcal{C} \circ \mathcal{D} \qquad (21)$$

$$\mathcal{R} : \begin{bmatrix} \phi_1^+ \\ \phi_2^+ \end{bmatrix}_n \rightarrow \begin{bmatrix} \phi_1^+ \\ \phi_2^+ \end{bmatrix}_{n+1} \qquad (22)$$

Both phase return maps can be determined analytically and thus yield a predictable in-contact and non-contact phase return map to evaluate collision-to-collision behavior for contact interacting oscillatory systems. This approach has been previously used to study the dynamics of hybrid systems such as hopping robots [27,28]. To analyze these maps, we will look for fixed points, where $\Delta\phi_{n+1} = \Delta\phi_n$. In a collision-to-collision map plot, these occur when the map crosses the line of slope one. Lastly, the stability of the fixed points can be determined by analyzing the slope (derivative) of the map, at the fixed point. When the magnitude of the derivative is less than unity, the fixed point is stable because deviations from the fixed point get smaller over time. Thus a stable phase synchronization behavior will have a fixed point at $\Delta\phi = 0$ with slope less than 1.

3.5. Experimental validation of proprioceptive synchronization

To test the modeling and analysis framework developed in the previous subsections, we performed experiments with two simple robotic joints. We mounted two Dynamixel servos (AX-12; Robotis) to a rigid platform with rigid 3D printed links attached (length 18 cm, height 5 cm, width 1.5 cm). We commanded the angular position of the motors to follow the control law described by Equation (3) with the sinusoidal proprioceptive feedback law as defined in the previous section. The robots were separated by a variable lateral distance Δy (which serves as δ in our previous simplistic model, Figure 1(a), and variable longitudinal distance Δx Figure 2(a)). As the robot joints oscillated back and forth they came into contact with each other and stopped moving during the contact. We measured the phase difference immediately before contact, ϕ_i^-, and the phase difference immediately after contact, ϕ_i^+, and constructed the experimental collision-to-collision return map. We similarly generated the analytical phase return map through numerical iteration of Equation (6). We define the phase difference at the nth collision as $\Delta\phi_n$, as the phase difference immediately at the beginning of the collision (i.e. $\Delta\phi_n = \phi_1^- - \phi_2^-$).

The evaluation of the collision-to-collision phase difference map describes the evolution of $\Delta\phi$ over time. Figure 2 illustrates the comparison of experimental and model prediction of the collision-to-collision return map for sinusoidal proprioceptive feedback and three values of gain $\gamma = [0.2, 0.4, 0.6]$. When robots are separated by a small lateral distance they will always converge to small $\Delta\phi \approx 0$ along the path of purple points and arrow line. The comparison between the experimental data (blue points) and the model predictions (red lines) is quite good across the three gains evaluated. These experiments indicate that contact interactions can potentially drive gait phase synchronization in undulatory robots.

In Figures 3 and 4, we perform experiments with variable lateral and longitudinal spacing. When the two robots are separated by a specific lateral distance, they can still demonstrate a convergence to a smaller $\Delta\phi$ than the initial phase difference. Again these experiments agree well with the numerical predictions from our modeling (Figure 3, blue points and red lines are data and model respectively). However, with non-zero lateral spacing ($\delta > 0$ in analysis, $\Delta y > 0$ in experiment) the robots will converge to a non-zero $\Delta\phi$ at which point they can no longer collide. This can easily be seen from Equation (5) in which non-zero δ yields phases for ϕ_i that have no contact solution. This property has been called compatibility in recent studies of undulatory synchronization [29].

In general, the model yields reasonable predictions of the experimental data in Figures 3 and 4. The model captures and predicts the phase convergence behavior as observed in experiment. As the proprioceptive gain is increased the experiment and the model converge to phase locking faster (lower slope of return map; Figure 3b–d). However, there are noticeable differences
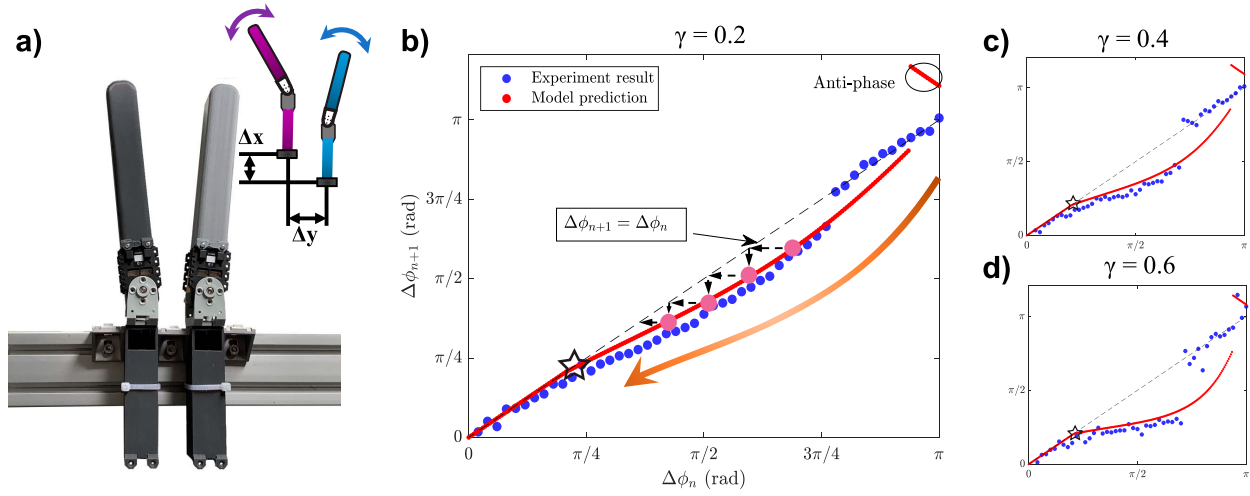
Figure 2. Experimental validation of phase convergence between contact-coupled oscillators. (a) Fixed body configuration: each robot comprises two rigid links with one oscillatory joint and one fixed bottom, laid out by predefined longitudinal and lateral separation distance $\triangle x$, $\triangle y$. (b) Contact return map from model prediction and experiment result with proprioceptive gain $\gamma = 0.2$ when $\triangle x = 0$ and $\triangle y = 0.02$ m. Red line are the theoretical solution by numerical integral for two oscillators. Black star indicates when the return map intercepts the unity slope line. Blue points are experimental phase states that two robots evolved to after collision from 50 sets of before-collision phase states. The purple points with the arrow line illustrate the trajectory of phase convergence between the intermittent contact. (c) and (d) The results of proprioceptive gain γ of 0.4 and 0.6.
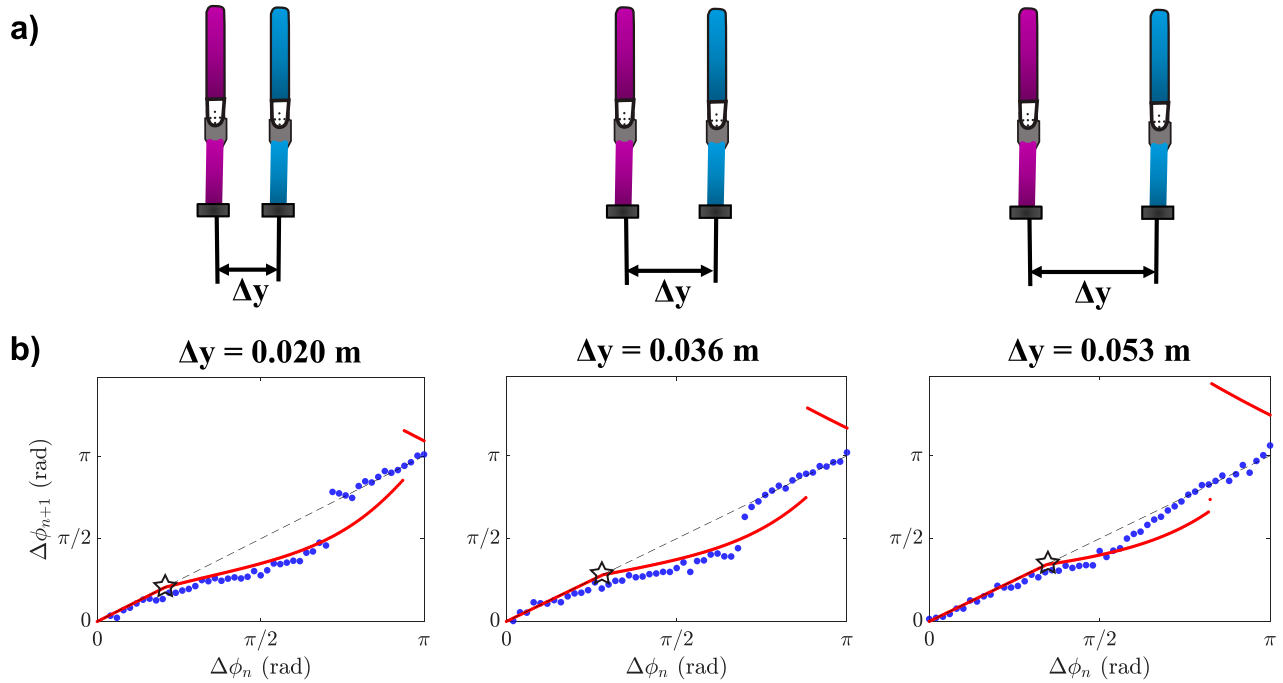

Figure 3. The effective adaption region differs from lateral separation: (a) spatial layouts for the robot pairs. $\triangle x = 0.0$ is fixed with varying $\triangle y = [0.020, 0.036, 0.053]m$ from left to right. (b) Phase return map. The compatible region (left bottom) and anti-phase region (top right) become larger with the increase of lateral distance.

between model and experiment. For example, in the experiments we notice a discontinuity in the experimental data points that occurs near $3\pi/4$ in Figure 3. We believe that this discontinuity is associated with the link geometry of the experiment (as compared to the 1D block model of Figure 1). When the links collide with each

other in the $\triangle\phi \approx \pi$ regime they push against each other with not just a normal contact force but also a tangential one. If the contact is not directly symmetric between the two links that may slip and the contact interaction is 'shorter' and wouldn't result in as much of a phase change (and thus $\triangle\phi$ for these slip interactions would like along
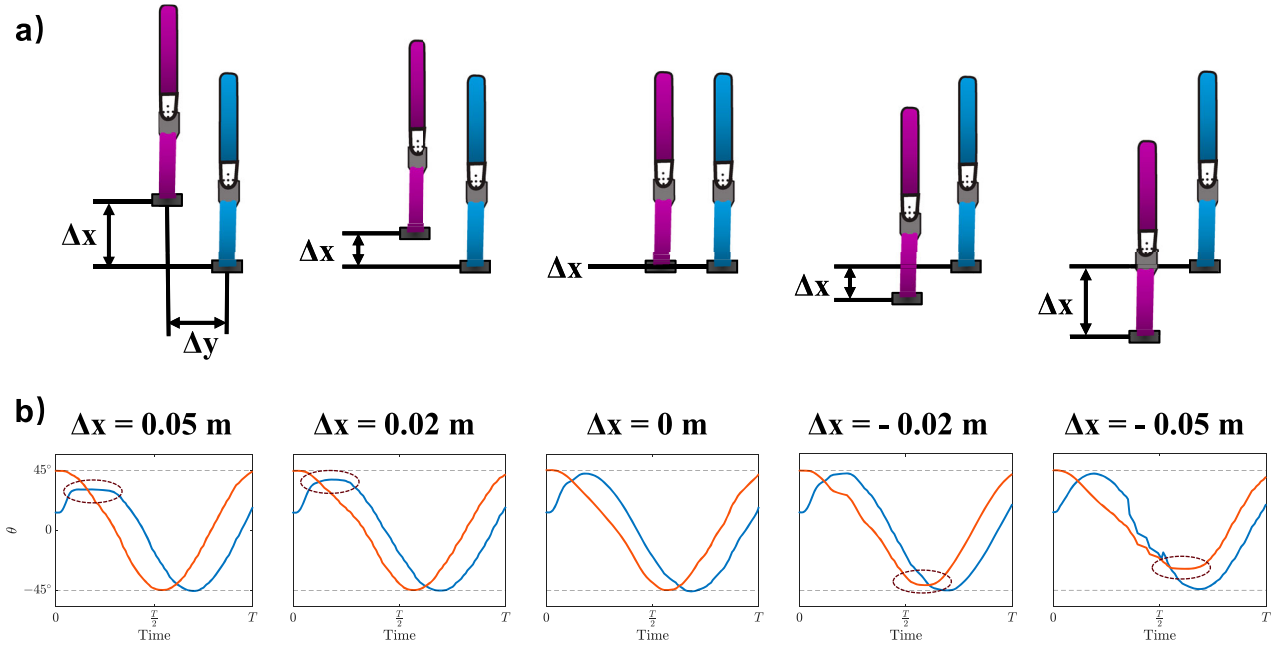
a)

b)

Figure 4. The phase adaption process varies with longitudinal separation. (a) Spatial layouts for the robot pairs. $\Delta y = 0.02m$ is fixed with varying $\Delta x = [0.05, 0.02, 0.00, -0.02, -0.05]m$ from left to right. (b) The joint angle adaption process within one period (single collision). The spatially behind robot can easily adapt the individual phase to the front one.

the 1 to 1 line). Further evidence of this can be seen in Figure 3 where this discontinuity is at a different angle when the width is changed (or non-existent for the widest case). These are practical issues that are not present in our simplistic toy model that we use to motivate the analysis of these systems.

Furthermore, when there is longitudinal separation between the robots the phase convergence behavior is altered from our simpler modeling in previous sections. Figure 4 shows that longitudinal separation Δx influences the interaction forces between the robots and thus the robot that is spatially behind the leading robot can more easily adapt the phase of the front robot because of the unbalanced moment of force. This spatial affect is not accounted for in our simple model and yet may complicate synchronization behavior in freely moving undulatory robots.

The modeling method of this work focused on a very narrow range of potential contact interactions. Our assumption that when the robots contact they come to rest is based on the following logic. There are in principal two types of collisions: (1) head on collisions like we model here where two robots collide with opposite sign commanded velocity and (2) rear end collisions in which the robots collide and potentially move together as you suggest with the same sign of commanded velocity. While it is possible for phase adaptation to occur in the rear end collisions, the phase change is much smaller per collision than in the case of the head on collisions. This is because

the robots are still able to move when in contact and thus there is not the large change between measured and controller phase that results in phase adaptation. However, the head on collisions result in large phase change because the robots come to rest during contact. We note that a rear end collision typically evolves to the case of a head on collision because while they move in contact eventually one of the robots reaches its turning point and reverses direction turning into a head on collision which results in both the robots stopping moving and coming to rest. Thus, while there may be many other types of collisional interactions that can occur, the head interactions are likely to result in the largest phase change and thus dominate the phase dynamics among the group.

4. Design principles of adaptive phase controller

In this next section, we now study the role of the proprioception feedback function on synchronizing the phases of undulatory gaits. We study this process using the collision-to-collision return map approach presented in previous sections.

4.1. Functional form influences synchronization

The proprioception function, $g(\phi_m, \phi)$, measures the difference between the measured phase and the controller phase. In the previous section, we used a trigonometric

Function	Mathematical expression
Sinusoidal	$\sin(\phi_m - \phi)$
Linear	$\mathrm{mod}\ (\phi_m - \phi + \pi,\ 2\pi) - \pi$
Tilted sinusoidal	$\sin(\phi_m - \phi + \sin(\phi_m - \phi - \frac{3}{4}))$
Exponential	$\mathrm{sign}(\ \mathrm{mod}\ (\phi_m - \phi + \pi,\ 2\pi) - \pi)(e^{\lvert\ \mathrm{mod}\ (\phi_m - \phi + \pi,\ 2\pi) - \pi\rvert} - 1)$

function $\sin(\phi_m - \phi)$ to modulate the internal phase of the toy model and the one-joint robot links. The periodicity and boundedness of the function guarantee a smooth phase evolution. However, the periodic nature of the feedback function results in a potential defect: the system has the same regulation effect for large ($\Delta\phi \to \pi$) and small ($\Delta\phi \to 0$) phase difference regions. This could potentially lead slower convergence to phase synchronization when initial phases are such that $\Delta\phi \approx \pi$. This issue can be resolved by taking alternative functional forms $g(\phi_m, \phi)$. In the table below, we list four functional forms of $g(\phi_m, \phi)$ that we will investigate in the context of phase synchronization: Figure 5(a) shows plots of these four functions versus phase difference.

4.2. Proprioceptive gain influences phase synchronization

We study the phase convergence properties of these four functions using the collision-to-collision return map (Figure 5b). The linear and exponential proprioceptive functions can dramatically change the convexity of return map curve, ensuring better faster convergence from large phase differences. Meanwhile, the tilted sinusoidal theoretically resolve the anti-phase fixed point that exists for the sinusoidal proprioceptive feedback.

The feedback adaptive function, $g(\phi_m, \phi)$, is multiplied by a single proprioceptive gain term γ. We hypothesize that the phase synchronization dynamics are dependent on the sign and magnitude of γ. Here we study the role of γ for the sinusoidal feedback function. Figure 5(c) shows that when $0 < \gamma < \omega$, we observe that oscillator phases always achieve synchronization and the magnitude of γ controls the shape of the collision-to-collision return map which in turn affects convergence speed. However, γ is restricted not to exceed ω, otherwise the synchronization dynamics break down because the oscillatory motion is no longer smooth. When $\gamma < 0$, the oscillator is driven to anti-phase synchronization as the $\Delta\phi = 0$ fixed point is no longer stable, while $\Delta\phi = \pi$ becomes stable. Figure 5(d) presents the stability of the $\Delta\phi = 0$ fixed point, which is calculated as the derivative of the collision-to-collision return map evaluated at $\Delta\phi = 0$. When the magnitude of the slope of the fixed point is less than unity, the fixed point is stable

because deviations from the fixed point get smaller over time. When the magnitude of the slope is greater than unity, the fixed point is unstable. This clearly shows how changing sign of γ changes the stability of in phase synchronization. When $\gamma = 0$, the gain puts the control into a pure feedforward form with no feedback, and the dynamics equations can be integrated to resolve the time-dependent actuation. With no feedback gain, the collision-to-collision return map is $\Delta\phi_{n+1} = \Delta\phi_n$ and the phase difference never changes.

5. Proprioceptive synchronization in three-link undulatory robots

5.1. Three-link robot design and control

A bio-inspired n-link robot can locomote through body undulations controlled by an oscillatory networks comprising $n-1$ actuated joints. The joint oscillations just require phase lag between neighbor links from head to tail that can yield a traveling wave of actuation. A complete travelling wave can be generated through a set of angles $\alpha_1, \alpha_2, \ldots, \alpha_{n-1}$, whose phases $\phi_1, \phi_2, \ldots, \phi_{n-1}$ uniformly distribute around one cycle, using the following equation:

$$\alpha_i = r_i \cos(\phi_i) \quad i = 1, 2, \ldots, n-1 \qquad (23)$$

where r_i and ϕ_i are governed by proposed collision-driven adaptive phase oscillator:

$$\dot{\phi}_i = \omega + \gamma g(\phi_{m,i}, \phi_i)$$
$$\dot{r}_i = r_i(\mu - r_i^2) \qquad (24)$$

The framework enables the phase adaption effect to emerge between different joints through collisions. For a single robot that does not contact any other robots, the joint–joint phase difference is held constant by the controller. However, when robots interact through contact the influence of the proprioceptive feedback can augment the traveling wave generation. It is challenging to retain a stable traveling wave under extreme collision scenarios because the adaption effect frequently perturbs the phase states. Therefore, as Figure 6, we introduce the inter-oscillator coupling and therefore transforming the oscillator system into a Central Pattern Generator (CPG) network as

$$\dot{\phi}_i = \omega + \gamma g(\phi_{m,i}, \phi_i) + \sum_{j=1}^{n} \lambda f(\phi_i, \phi_j)$$
$$\dot{r}_i = r_i(\mu - r_i^2) \qquad (25)$$

In Equation (25), the adaptive function $g(\phi_{m_i}, \phi_i)$ of proprioceptive gain $\gamma \in [0, \omega]$ is employed to enable
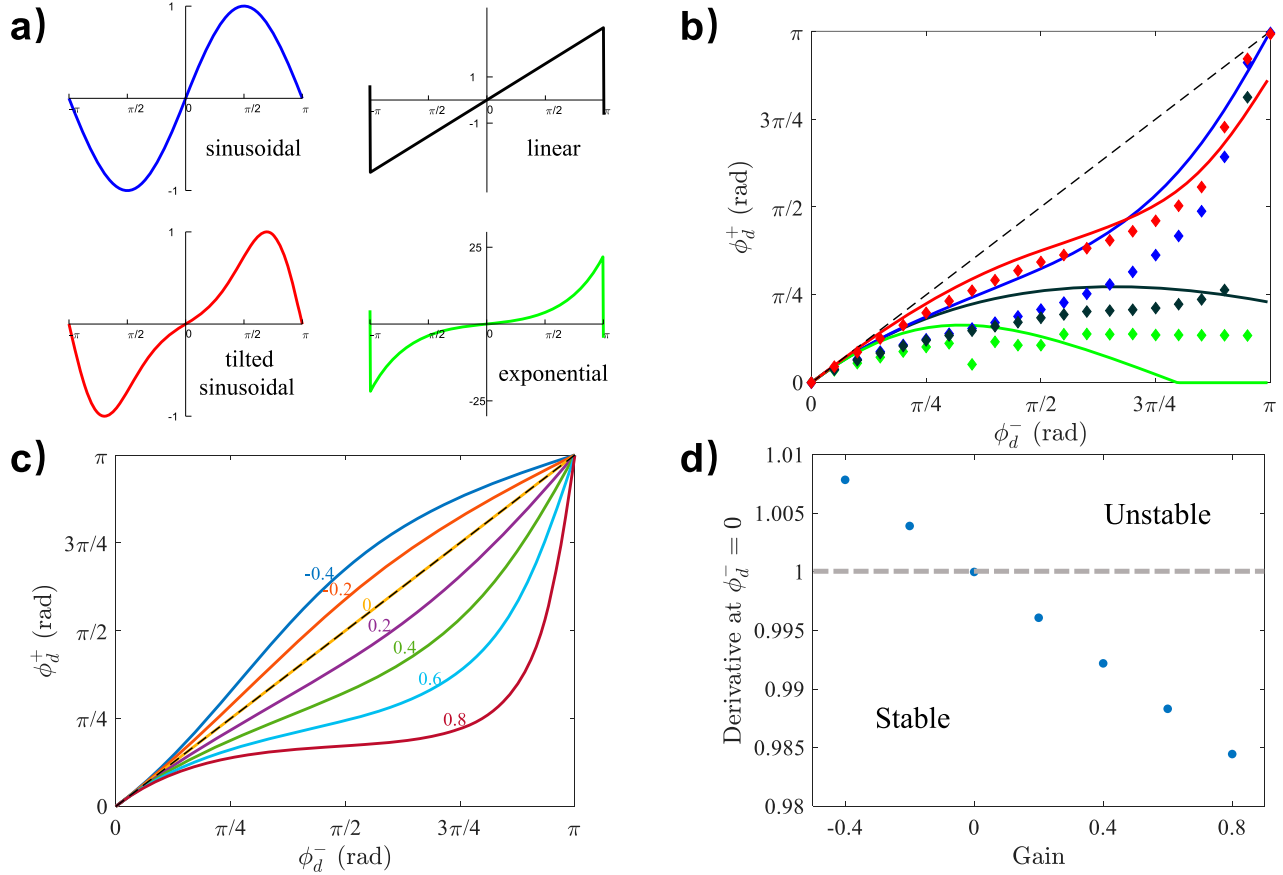
Figure 5. Proprioceptive feedback design changes the convergence of the contact return map. (a) Demonstration of adaptive function on $[-\pi, \pi]$. (b) Adaptive function $f(\Delta\phi)$ changes the convexity of contact return map. Different colors stand for different forms of the adaptive function: blue – sinusoidal, red – tilted sinusoidal, dark – linear, and green – symmetric exponential (see details on (a)). The functions are all symmetrical around the origin with period $T = 2\pi$. The diamond points are simulation results, which are well matched with the respective prediction curves. (c) The sign and magnitude of proprioceptive gain γ. When $0 < \gamma < \omega$, two oscillators synchronize to in-phase status, the magnitude of γ controls the speed of the synchronization process. When $\gamma < 0$, the oscillators are driven to the anti-phase synchronization. When $\gamma = 0$, the oscillators evolve as time-dependent actuation without synchronization. (d) Convergence rate at $\phi_d^- = 0$ versus gain values.

phase synchronization. The function $f(\phi_i, \phi_j)$, a.k.a. the CPG function, with inter-CPG couplings $\lambda \in [0, 1]$, governs the traveling wave pattern through the internal phase regulation among joints. The form of the functions can be considered as

$$g(\phi_{m,i}, \phi_i) = \sin(\phi_{m,i} - \phi_i)$$
$$f(\phi_i, \phi_j) = \sin(\phi_j - \phi_i - \psi) \qquad (26)$$

where the phase offset ψ controls the relative phase difference between adjacent joints. In our setup, ψ is chosen to realize the specific motion pattern, i.e. sinusoidal wave along longitudinal body for three-link robot ($\psi = \frac{2\pi}{3}$) and four-link robot ($\psi = \frac{\pi}{2}$). We implement this control structure in experiments and simulations of three-link robots. The geometry of the robots is shown in Figure 7(a). In experiment we use two Dynamixel AX-12 motors as the joints, controlled through position commands. We also simulate these systems in PyBullet using

similar geometry as in experiment, and joints that are controlled through position commands.

5.2. Space and phase dynamics in channel traversal

In our first experiments and simulation, we study how multiple robots in confinement can reach phase synchronization through contact. In simulation, two three-link robots are placed inside a parallel channel which limits how far they can be pushed away from each other and which enforces collision interactions (Figure 7b). They are initialized with specific phases and center positions. The channel width CW and proprioceptive gain γ vary from 0.11 m to 0.13 m and 0 to 1, respectively. The relative lateral separation distance Δx and phase difference $\Delta\phi$ are collected to generate swarm configuration. For the robot pair system, Δx and $\Delta\phi$ precisely describe the dynamic difference in spatial and phase dimensions.
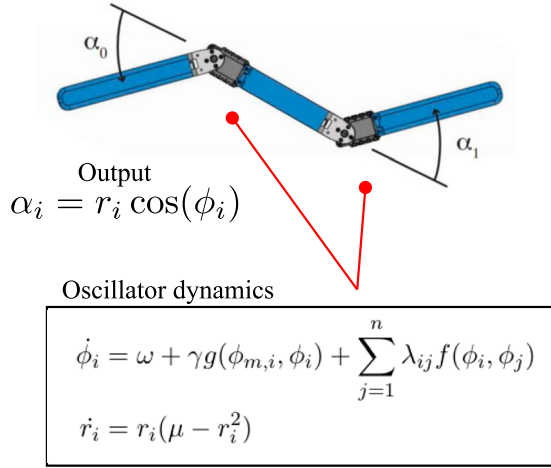
Figure 6. Control scheme for the single multi-link robot.

We define the return map of the robot pair system $\mathcal{M}$ as

$$\mathcal{M} : \begin{bmatrix} \phi_1^+ \\ \phi_2^+ \\ \Delta x^+ \end{bmatrix}_n \rightarrow \begin{bmatrix} \phi_1^+ \\ \phi_2^+ \\ \Delta x^+ \end{bmatrix}_{n+1} \qquad (27)$$

which is equivalent to

$$\mathcal{M} : (\Delta\phi^- = \phi_1^- - \phi_2^-, \Delta x^-)$$
$$\rightarrow (\Delta\phi^+ = \phi_1^+ - \phi_2^+, \Delta x^+) \qquad (28)$$

Figure 7(c) shows that in simulation three different steady-state configurations of spatial shift (Δx) and phase shift ($\Delta\phi$) emerge from the synchronization process. We find that simulations at varying initial Δx and initial $\Delta\phi$ cluster along a stair-stepped curve. Overall the steady states that emerge converge to the three compatible regions along the gradient of the heatmap, one link ahead, in-phase, and one link behind states. When the gain is set to zero no phase change can occur and we see that the robots populate the central curve by adjusting Δx based on $\Delta\phi$. This central curve is called the compatibility curve [30]. The bottom-middle and bottom-right panels in Figure 7(c) verify that gain and channel width can help increase the attraction of compatible regions.

5.3. Proprioceptive gain determines the collective locomotion pattern

We next study how larger groups of robots are capable of synchronizing their gaits (Figure 8). In these experiments, we used four robots placed in a channel of width 0.22 m. The robots were actuated given by Equation (25) as introduced in the previous section. We used a sinusoidal proprioceptive feedback function and we varied the gain, γ. The robots were initiated at one end of the channel with the same longitudinal positioning across all robots.
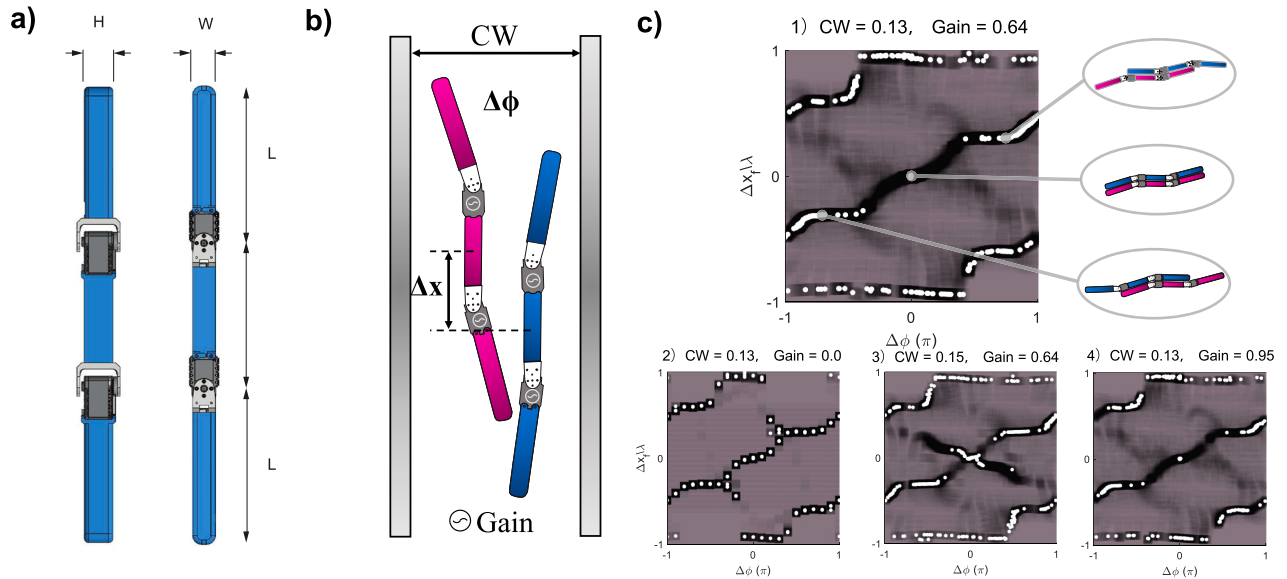

Figure 7. The compatible configuration is associated with channel width and proprioceptive gain, γ. (a) Robot geometry parameter illustration. b) Simulations are performed with two robots in a narrow channel of channel width, CW. Robot pairs may achieve gait compatibility through contact-driven spatial translation and phase adjustment in the confined space. (c) A heat map of observed probability density from simulations starting at different lateral separation $\Delta x/\lambda$ versus kinematic phase difference $\Delta\phi$. Darker areas correspond to a higher probability of observation in that state. White points indicate the final states of the two robots after 150 periods of oscillation. The simulation was performed under different channel width and gain ($= \frac{\gamma}{\omega}$) conditions 1–4. The initial setup of the simulations is taken from every grey gird point in the map, i.e. $\Delta x/\lambda = -1{:}0.1{:}1$, $\Delta\phi = -\pi{:}0.1\pi{:}\pi$.
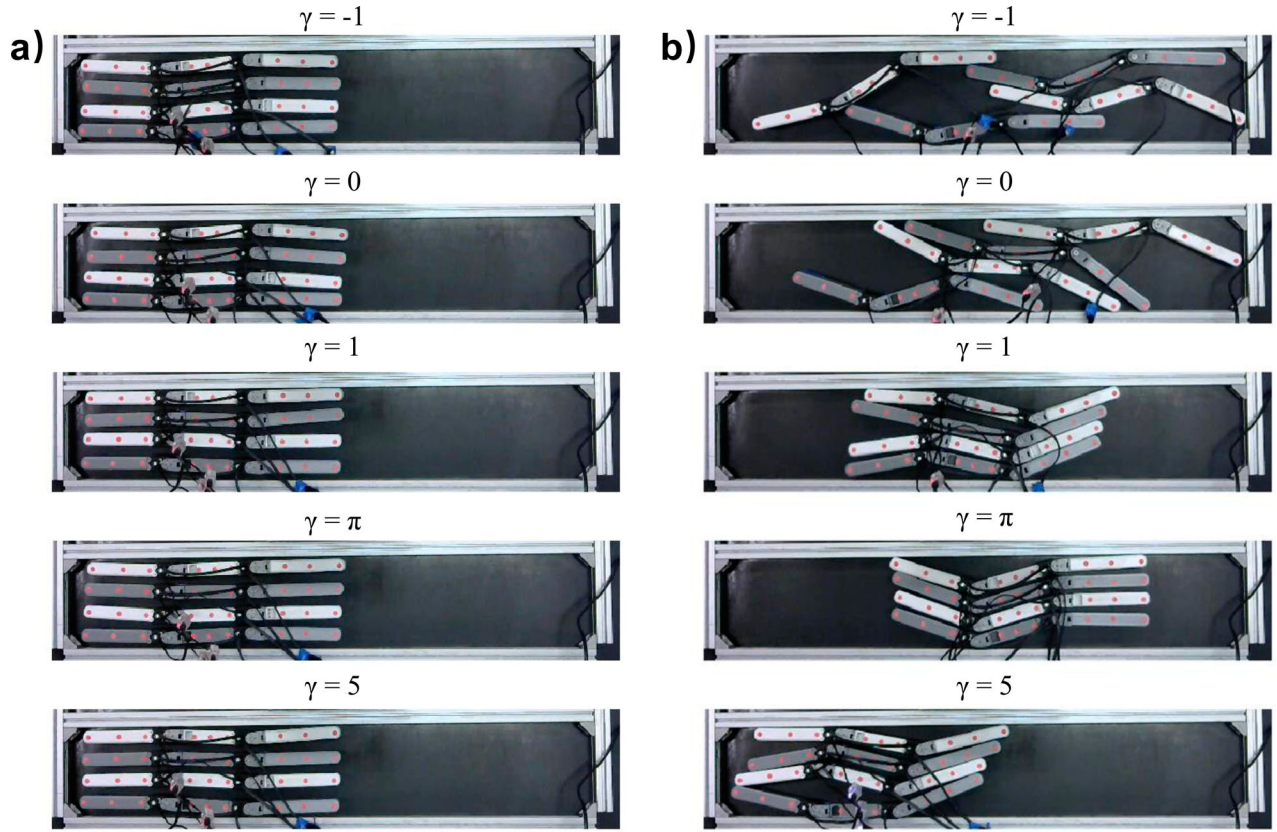
Figure 8. Collective behaviors hinge upon adaptive coefficient γ. (a) Robot groups are actuated with the same intrinsic frequency $\omega = \pi$ but different adaptive coefficient $\gamma = [-1, 0, 1, \pi, 5]$ from top to bottom. (b) The steady motion pattern (from top to bottom): disordered motion, compatible motion, partial synchronized motion, complete synchronized motion, and suppressed motion.

In our first experiments, we set the feedback gain to $\gamma = -1$ which in analysis leads to anti-phase synchronization. We did not find that the robot group achieved perfect anti-phase synchronization, but instead the robots exhibited controller phases that diverged and drifted over a large range during the experiment. It is likely that the mobility of the robots, as they could push each other away spatially, disrupts the anti-phase synchronization process and leads more general disordered undulations among the group.

When the proprioceptive feedback was turned off $\gamma = 0$ the robots pushed against each other and shifted their longitudinal positioning to achieve a configuration which allowed them to oscillated indefinitely. The lack of phase adaptation in these experiments meant that every situation was different depending on the random initial phases chosen.

When the feedback gain was less than the oscillator frequency ($\gamma < \omega$; $\omega = \pi$) the robot group was capable of producing collective in-phase behavior robustly. Figure 8(b) shows the final configurations of the four robots in which for $\gamma = 1, \pi$ the robots achieve final synchronized group motion despite starting from very different initial phases. The larger gain experiments produced faster convergence to synchronization.

Lastly, we studied what happens when $\gamma > \omega$ in experiments with four robots. In these experiments, the joints failed to oscillate smoothly and instead in many experiments locked or halted motion. This is likely because even small noise from the proprioceptive feedback function is amplified significantly by the gain term, and thus leads to spurious oscillatory dynamics.

5.4. Synchronization enhance channel traversal ability

In this last section, we study how synchronization of gaits can improve the collective locomotion performance of undulatory robots. We first performed simulations of robot pairs moving in a channel of width 0.095 m (Figure 9a) and moving under the influence of a simulated viscous fluid force (i.e. swimming at low Reynolds number [31]). To establish a baseline for performance without proprioception, we fixed the robot pairs at a constant phase difference between 0 and π and measured the time to traverse a distance of 0.8 m along the
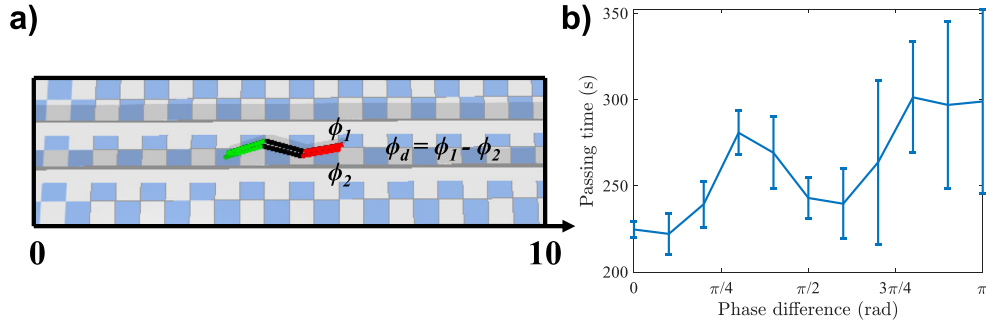
Figure 9. Channel traversal efficiency. (a) Simulation configuration of robot pair. Phase difference is fixed in the process. (b) Simulation results show that in-phase robot pairs always perform regular and high-speed swimming. The fine points record the average time cost of two robots for swimming 0.8 m length channel with different phase difference.
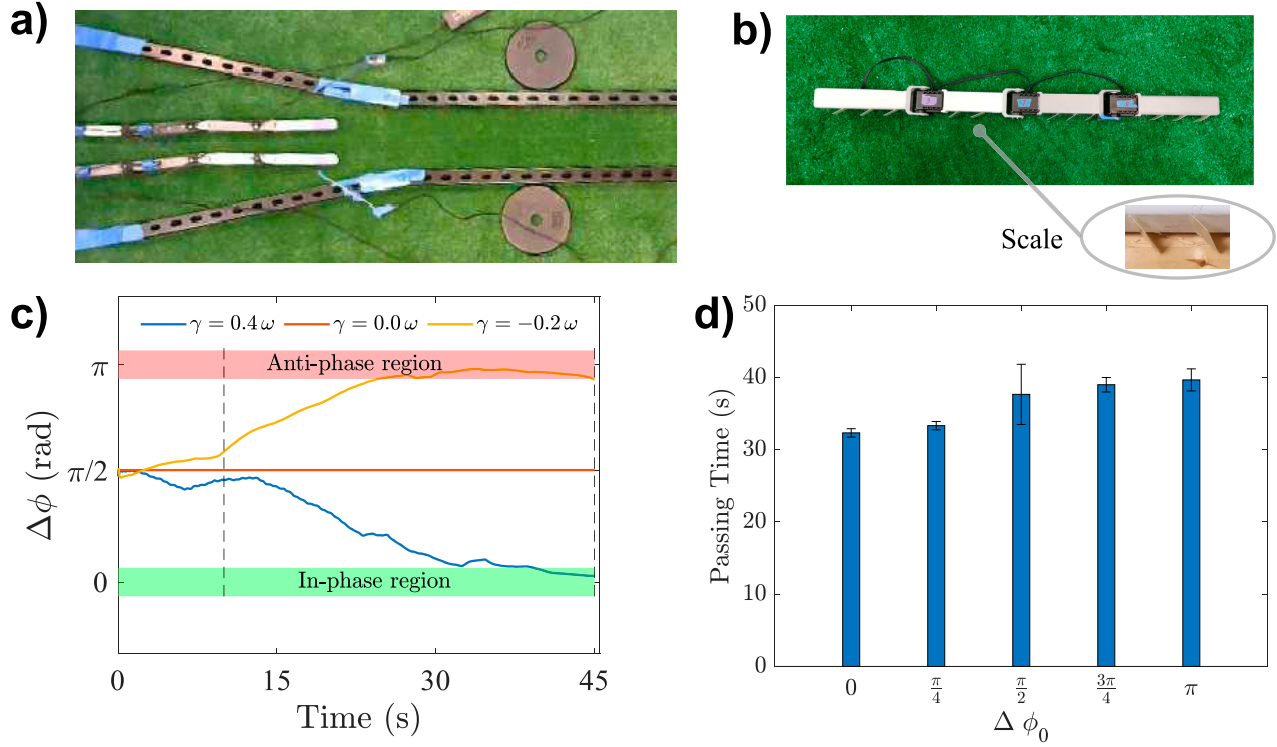

Figure 10. Robot pairs passability. (a) An overhead picture of two robots challenged to move through a narrow channel. (b) Scale appendages on bottom surface provide anisotropic friction interacting with grass ground. (c) Relative phases between the two robot showing: in-phase synchronization at $0 < \gamma < \omega$, anti-phase synchronization at $\gamma < 0$, and non-feedback at $\gamma = 0$. (d) The synchronization status of robot pairs take effect on the moving efficiency. Synchronized pairs initialized with gain $= 0.3$ and $\Delta \phi_0$ ranging from 0 to π cost increasing time to travel the 0.5m length channel.

channel length. We observe that the passing time non-monotonically increased from phase differences of 0 to π. Importantly, the smallest phase differences $(0 - \pi/8)$ exhibited the shortest traversal time compared to other phase differences. Thus synchronization of robot gaits can improve locomotion speed of robot pairs when in confined environments.

We experimentally test whether robot gait synchronization can improve performance when two robots are challenged to pass through a narrow channel together. To enable the robots to locomote forward we

performed these experiments on an artificial grass surface (Figure 10a), and we placed angled plastic beams as the scale appendages on the bottom of the robots body to generate anisotropic friction (Figure 10b). The scales ensure the robot can move forward longitudinally through the interaction with the grass. For stability we added an extra joint and link to these robots making them four-link snake-like robots. We used a similar control method as described above in Equations (25) and (26), i.e. $\psi = \frac{3\pi}{4}$, $\lambda = 0.4$. The channel the robots were to traverse was formed from steel beams that angled from

a wider spacing to a narrow constriction of 0.21 m in width. The robots were placed in the wider entrance and were separated laterally and aligned longitudinally. During the first motion stage (around first 10 seconds), the robots moved in the wider space and the phase adaption through contact did not significantly impact the robot phases (time before dashed line in Figure 10 c). However, when traversing the narrow channel (time after dashed line in Figure 10(c), the two robots start to interact more significantly through contact and influence each other's phase through proprioceptive feedback. In Figure 10(c), we show three examples of phase change versus time for a positive, negative, and zero proprioceptive gain. As expected based on our previous modeling and experiments the robots synchronized to in phase or anti-phase behavior based on the sign of γ. These experiments illustrate that phase adaption and convergence effect were influenced by two factors: (a) channel width influences whether the robots can robustly interact with each other which is required to achieve synchronization and (b) the sign of the proprioceptive gain determines the ultimate synchronization capability of the robots.

To validate the beneficial role of gait synchronization, we performed separate experiments in which the robots were held at a fixed phase difference (i.e. $\gamma = 0$) and we measured the time duration for the robots to completely pass through the channel. We observed a modest decrease in the traversal time for the synchronized robots ($\Delta\phi = 0$; Figure 10 d) and a longer traversal time for larger phase differences. These experimental results are in accord with the simulation results discussed previously (Figure 9).

6. Discussion

In this study, we demonstrated that undulatory motion in biologically inspired robots can be synchronized through contact interactions without the need for robot-robot communication. By designing appropriate proprioceptive feedback into a robot's undulatory controller we are able to generate emergent synchronized motion. The shape of the collision-to-collision return map hinges on the proprioceptive gain and proprioceptive function. Proprioceptive feedback inspired from neuromechanical studies of *C. elegans* enable emergent phase synchronization and determine the pattern of collective behaviors. Robot pairs that traverse narrow channels can synchronize their gait to move effectively together in confined space. Overall, these results suggest new methods for designing feedback control of emergent phase synchronization in a robot swarm.

The synchronization of coupled oscillator systems has a long and rich history in nonlinear dynamics, robotics,

and neuroscience [24]. However, these systems are typically coupled directly through the control system or dynamical equations of motion. For example, as mentioned in Section 2 the Kuramoto model of synchronization relies on direct 'sharing' of oscillator phase information between oscillators. More recently, examples of oscillator coupling that occurs through self-motion of the body have demonstrated synchronization and entrainment of undulatory gaits. For example, 'reflexive' like behaviors in snake robots that respond to local body bending curvature can generate emergent locomotor gaits [32]. Coupling such oscillators with external force sensors that respond to hydrodynamic body forces can similarly organize coordinated and coupled body motion in a swimming robot [33]. The design of emergent locomotor gaits through mechanical coupling and active actuation responses is an area of great interest for future adaptive robots. Furthermore, the study of bio-inspired robots that emulate principles from their living systems counterparts can provide new insights into biology [34].

In this work, we propose to solely use proprioceptive information for coordinating motion among robots. In similar work, Sato et al. [35] have developed a method of generating adaptive undulatory locomotion through a 'discrepancy function' which is quite similar to the proprioceptive feedback in the work presented here. The discrepancy function of Sato et al. monitors the joint error of an undulatory snake robot and produces an adaptive phase through a simple differential equation between the discrepancy function and phase adaptation. The addition of other internal state variables, such as this discrepancy function, may greatly expand the robustness of the phase synchronization process and the speed of adaptation. This will be of great interest in future studies of contact-mediated robot coordination.

In addition, by adding extra state variables to the control system one can potentially enable a broader range of synchronization phenomena. For example, in the work studied here all robots had the same intrinsic oscillator frequency. Yet arguably the most striking examples of synchronization are among oscillator populations with different intrinsic frequencies (as in the case of the classic Kuramoto system [25]). Thus it will be interesting to determine how robust the method proposed here is to frequency variation. If the frequency synchronization among undulatory robots is not possible with the current methods, one may look to additional control elements such as the discrepancy function [35] or adaptive oscillators [36,37].

Collective systems that interact through contact have been extensively studied in the physics of granular

materials [38] and active matter [39]. The emergent properties of these systems, such as clustering for example [39], may present unique opportunities for control of multi-robot systems. From the physics community there has been recent interest in the emergent dynamics of simple, 'active' robots that interact through contact [40,41]. Similarly, from the swarm robotics community there has been recent interest in leveraging contact and collisional interactions as a means of coordinating robot group behaviors [42–47]. Typically in this previous work only repulsive normal force contacts have been considered. However, there has been recent interest in cohesive interactions between robots through magnets [48] or shape interlocking (called entanglement) [49]. For example, a recent studied inspired by the collective behavior of blackworms has demonstrated how mechanical entanglement and coordinated movement between simple robots can allow the group to move collectively along temperature gradients [50].

This work represents a first examination of how intermittent contact can be used for information exchange and designed emergent behaviors. Future work will explore how more complex group behaviors such as turning, clustering/expanding, and group sensing can be enabled by contact mediated 'communication'. Similarly, examination of how limit-cycle motion generation can lead to more complex gait behaviors. For example how more complex dynamical attractors can yield gaits that are modified when in the presence of other robots and in complex environments. More broadly, the convergence of physics, dynamics, and robotics represents an exciting new direction for discovering and controlling emergent phenomena [51].

Disclosure statement

No potential conflict of interest was reported by the author(s).

Notes on contributors

Zhuonan Hao received his B.S. degree in Vehicle Engineering from Beijing Institute of Technology in China, and M.S. degree in Mechanical Engineering from the University of California, San Diego. His Master's thesis was entitled Design Principles for Locomotion Synchronization in Undulatory Robot Groups. He is currently a PhD student in the Structure–Computer Interaction lab at the University of California, Los Angeles. His interests and research are in the areas of bio-inspired soft robotics.

Wei Zhou received his B.S. degree in Mechanical Engineering and Automation from Beihang University and Master's degree in Mechanical Engineering from the University of Michigan Ann Arbor. He is currently a PhD student in the Gravish Lab in the Mechanical & Aerospace Engineering department at the University of California, San Diego. His interests and research are in the areas of control & dynamics and robotics.

Nick Gravish received his B.S. degree in Physics from the University of California, Santa Barbara in 2005. He received his PhD from the Georgia Technology Institute in the Department of Physics in 2013. From 2013 to 2016, he was a post-doc in the Harvard microrobotics lab and the Combes insect flight lab where he developed bioinspired robots and methods for insect biomechanics study. He is currently an assistant professor in the Mechanical & Aerospace Engineering department at the University of California, San Diego, where he joined in 2016. In 2013, Dr. Gravish was selected as a McDonnell fellow in Complex Systems Science and in 2020 he received a CAREER award from the National Science Foundation. His research interests lie the areas of Animal Biomechanics, Robotics Inspired Biology, and Robophysics study of nonlinear dynamical systems. These areas intersect in the study of robot and animal locomotion which are studied in his lab at UC San Diego.

ORCID

Zhuonan Hao http://orcid.org/0000-0001-5256-8528
Wei Zhou http://orcid.org/0000-0001-7707-4022
Nick Gravish http://orcid.org/0000-0002-9391-2476

References

[1] Brambilla M, Ferrante E, Birattari M, et al. Swarm robotics: a review from the swarm engineering perspective. Swarm Intelligence. 2013 Mar;7(1):1–41.

[2] Gueron S, Levit-Gurevich K, Liron N, et al. Cilia internal mechanism and metachronal coordination as the result of hydrodynamical coupling. Proc Natl Acad Sci. 1997;94(12):6001–6006.

[3] Wollin C, Stark H. Metachronal waves in a chain of rowers with hydrodynamic interactions. European Phys J E. 2011;34(4):3–10.

[4] Button B, Cai L-H, Ehre C, et al. A periciliary brush promotes the lung health by separating the mucus layer from airway epithelia. Science. 2012;337(6097):937–941.

[5] Gopinath A, Mahadevan L. Elastohydrodynamics of wet bristles, carpets and brushes. Proc Royal Soc A Math Phys Eng Sci. 2011;467(2130):1665–1685.

[6] Elgeti J, Gompper G. Emergence of metachronal waves in cilia arrays. Proc Natl Acad Sci USA. 2013 Mar;110(12):4470–4475.

[7] Elfring GJ, Lauga E. Hydrodynamic phase locking of swimming microorganisms. Phys Rev Lett. 2009 Aug;103(8):088101.

[8] Yuan J, Raizen DM, Bau HH. Gait synchronization in caenorhabditis elegans. Proc Natl Acad Sci USA. 2014 May;111(19):6865–6870.

[9] Chelakkot R, Hagan MF, Gopinath A. Synchronized oscillations, traveling waves, and jammed clusters induced by steric interactions in active filament arrays. Soft Matter. 2020 Dec;17:1091–1104.

[10] Quillen AC, Peshkov A, Wright E, et al. Metachronal waves in concentrations of swimming turbatrix aceti nematodes and an oscillator chain model for their coordinated motions. Phys Rev E. 2021 Jul;104(1):014412.

[11] Fang-Yen C, Wyart M, Xie J, et al. Biomechanical analysis of gait adaptation in the nematode caenorhabditis elegans. Proc Natl Acad Sci. 2010;107(47):20, 323–20, 328.

[12] Wen Q, Po MD, Hulme E, et al. Proprioceptive coupling within motor neurons drives *C. elegans* forward locomotion. Neuron. 2012 Nov;76(4):750–761.

[13] Ji H, Fouad AD, Teng S, et al. Phase response analyses support a relaxation oscillator model of locomotor rhythm generation in *Caenorhabditis elegans*. Elife. 2021 Sep;10:e69905.

[14] Buchli J, Righetti L, Ijspeert AJ. Engineering entrainment and adaptation in limit cycle systems. Biol Cybern. 2006;95(6):645–664.

[15] Strogatz SH. Nonlinear dynamics and chaos: with applications to physics, biology, chemistry and engineering. Boulder, CO: Westview Press; 2000.

[16] Righetti L, Buchli J, Ijspeert AJ. Adaptive frequency oscillators and applications. Open Cybern Systemics J. 2009;3(1).

[17] Ceron S, Kimmel MA, Nilles A, et al. Soft robotic oscillators with strain-Based coordination. IEEE Robotics Automat Lett. 2021;6:7557–7563.

[18] Jouaiti M, Hénaff P. Comparative study of forced oscillators for the adaptive generation of rhythmic movements in robot controllers. Biol Cybern. 2019 Dec;113(5-6):547–560.

[19] Dutta S, Parihar A, Khanna A, et al. Programmable coupled oscillators for synchronized locomotion. Nat Commun. 2019 Jul;10(1):3299.

[20] Garcia M, Chatterjee A, Ruina A, et al. The simplest walking model: stability, complexity, and scaling. J Biomech Eng. 1998 Apr;120(2):281–288.

[21] Asano F. Efficiency and optimality of two-Period limit cycle walking. Adv Robot. 2012 Jan;26(1-2):155–176.

[22] Solomon JH, Wisse M, Hartmann MJZ. Fully interconnected, linear control for limit cycle walking. Adapt Behav. 2010 Dec;18(6):492–506.

[23] Righetti L, Buchli J, Ijspeert AJ. Dynamic hebbian learning in adaptive frequency oscillators. Physica D Nonlinear Phenomena. 2006;216(2):269–281.

[24] Pikovsky A, Kurths J, Rosenblum M, et al. Synchronization A universal concept in nonlinear sciences. Cambridge: University Press; 2003.

[25] Kuramoto Y. Chemical oscillations, waves, and turbulence. Berlin, Heidelberg: Springer; 1984.

[26] Acebron JA, Bonilla LL, Vicente CJP, et al. The Kuramoto model: A simple paradigm for synchronization phenomena. Rev Mod Phys. 2005 Jan;77(1):137–185.

[27] Koditschek DE, Buehler M. Analysis of a simplified hopping robot. J Robot Res. 1991;10:587–605.

[28] Holmes P, Full RJ, Koditschek D, et al. The dynamics of legged locomotion: models, analyses, and challenges. SIAM Rev. 2006;48(2):207–304.

[29] Zhou W, Hao Z, Gravish N. Collective synchronization of undulatory movement through contact. Phys Rev X. 2021 Sep;11:031051. Available from: https://link.aps.org/doi/10.1103/PhysRevX.11.031051.

[30] Zhou W, Dezha-Peralta J, Hao Z. Synchronized swimming: collisions drive gait compatibility in undulatory robots. 2020.

[31] Hatton RL, Choset H. Geometric swimming at low and high Reynolds numbers. IEEE Trans Robot. 2013;29(3):615–624.

[32] Kano T, Sato T, Kobayashi R, et al. Local reflexive mechanisms essential for snakes' scaffold-based locomotion. Bioinspir Biomim. 2012 Dec;7(4):046008.

[33] Thandiackal R, Melo K, Paez L, et al. Emergence of robust self-organized undulatory swimming based on local hydrodynamic force sensing. Sci Robot. 2021;6(57): eabf6354. Available from: https://www.science.org/doi/abs/10.1126/scirobotics.abf6354.

[34] Gravish N, Lauder GV. Robotics-inspired biology. J Exp Biol. 2018 Mar;221(Pt 7):13828.

[35] Sato T, Kano T, Ishiguro A. On the applicability of the decentralized control mechanism extracted from the true slime mold: a robotic case study with a serpentine robot. Bioinspir Biomim. 2011 Jun;6(2):026006.

[36] Buchli J, Iida F, Ijspeert AJ. Finding resonance: Adaptive frequency oscillators for dynamic legged locomotion. 2006 IEEE/RSJ International Conference on Intelligent Robots and Systems; 2006 Oct. p. 3903–3909.

[37] Petrič T, Gams A, Ijspeert AJ, et al. On-line frequency adaptation and movement imitation for rhythmic robotic tasks. Int J Rob Res. 2011 Dec;30(14):1775–1788.

[38] Jaeger HM, Nagel SR, Behringer RP. Granular solids, liquids, and gases. Rev Mod Phys. 1996;

[39] Ramaswamy S. The mechanics and statistics of active matter. Annu Rev Condens Matter Phys. 2010 Aug;1(1): 323–345.

[40] Chvykov P, Berrueta TA, Vardhan A, et al. Low rattling: a predictive principle for self-organization in active collectives. Science. 2021 Jan;371(6524):90–95.

[41] Savoie W, Berrueta TA, Jackson Z, et al. A robot made of robots: emergent transport and control of a smarticle ensemble. Sci Robot. 2019 Sep;4(34):20120637.

[42] Mondada F, Gambardella LM, Floreano D, et al. The cooperation of swarm-bots: physical interactions in collective robotics. IEEE Robot Autom Mag. 2005 Jun;12(2):21–28.

[43] Mayya S, Pierpaoli P, Nair G, et al. Localization in densely packed swarms using interrobot collisions as a sensing modality. IEEE Trans Rob. 2019 Feb;35(1):21–34.

[44] Mayya S, Wilson S, Egerstedt M. Closed-loop task allocation in robot swarms using inter-robot encounters. Swarm Intelligence. 2019 Jun;13(2):115–143.

[45] Mayya S, Notomista G, Shell D. Non-uniform robot densities in vibration driven swarms using phase separation theory. 2019 IEEE/RSJ International Conference on Intelligent Robots and Systems (IROS); 2019 Nov. p. 4106–4112.

[46] Schmickl T, Thenius R, Moeslinger C, et al. Get in touch: cooperative decision making based on robot-to-robot collisions. Auton Agent Multi Agent Syst. 2009;18(1):133–155.

[47] Karimi MA, Alizadehyazdi V, Busque B. A Boundary-constrained swarm robot with granular jamming. 2020 3rd IEEE International Conference on Soft Robotics (RoboSoft); 2020 May. p. 291–296.

[48] Li S, Dutta B, Cannon S, et al. Programming active cohesive granular matter with mechanically induced phase changes. Sci Adv. 2021 Apr;7(17).

[49] Gravish N, Franklin SV, Hu DL, et al. Entangled granular media. Phys Rev Lett. 2012 May;108(20):208001.

[50] Ozkan-Aydin Y, Goldman DI, Bhamla MS. Collective dynamics in entangled worm and robot blobs. Proc Natl Acad Sci. 2021;118(6):357.

[51] Aguilar J, Zhang T, Qian F, et al. A review on locomotion robophysics: the study of movement at the intersection of robotics, soft matter and dynamical systems. Rep Prog Phys. 2016 Nov;79(11):110001.